

A Two-Parameter Matching Scheme for Massive Galaxies and Dark Matter Haloes

Andrea Kulier^{1*} and Jeremiah P. Ostriker^{1,2}

¹*Department of Astrophysical Sciences, Princeton University, Princeton, NJ 08544, USA*

²*Department of Astronomy, Columbia University, NYC, NY 10027, USA*

4 November 2021

ABSTRACT

Halo Abundance Matching has been used to construct a one-parameter mapping between galaxies and dark matter haloes by assuming that halo mass and galaxy luminosity (or stellar mass) are monotonically related. While this approach has been reasonably successful, it is known that galaxies must be described by at least two parameters, as can be seen from the two-parameter Fundamental Plane on which massive early-type galaxies lie. In this paper, we derive a connection between initial dark matter density perturbations in the early universe and present-day virialized dark matter haloes by assuming simple spherical collapse combined with conservation of mass and energy. We find that $z = 0$ halo concentration, or alternatively the inner slope of the halo density profile α , is monotonically and positively correlated with the collapse redshift of the halo. This is qualitatively similar to the findings of some previous works based on numerical simulations, with which we compare our results. We then describe how the halo mass and concentration (or inner slope α) can be used as two halo parameters in combination with two parameters of early-type galaxies to create an improved abundance matching scheme.

Key words: galaxies: haloes — galaxies: evolution — galaxies: formation — dark matter — cosmology: theory

1 INTRODUCTION

Halo abundance matching is one of several methods used to link galaxies with dark matter haloes. It uses the simple assumption that galaxy luminosity (or stellar mass) and halo mass are monotonically related, such that more luminous galaxies reside in more massive haloes, to match observed magnitude-limited samples of galaxies to dark matter halo merger trees from dark matter-only simulations (Vale & Ostriker 2004a; Kravtsov et al. 2004; Vale & Ostriker 2004b; Guo et al. 2010). Despite the simplicity of its underlying assumption, abundance matching is able to reproduce with surprising accuracy various measures related to the observed physical distribution of galaxies, such as the luminosity functions of different cosmic environments, the occupation numbers of haloes (Vale & Ostriker 2004a), galaxy autocorrelation functions (Conroy et al. 2006; Guo et al. 2010; Nuza et al. 2013), and galaxy-galaxy lensing (Hearin et al. 2013; Fosalba et al. 2015).

Being able to match large samples of galaxies and haloes without the use of complex semi-analytic or numeri-

cal hydrodynamic modeling has allowed for a simple probe of the connection between galaxies and their dark matter haloes. Abundance matching has been used to obtain various statistical relationships between galaxies and their host halos, such as the luminosity-halo mass and stellar-halo mass relations (Vale & Ostriker 2004b; Shankar et al. 2006; Conroy & Wechsler 2009; Behroozi et al. 2010; Guo et al. 2010; Wake et al. 2011; Leauthaud et al. 2012; Moster et al. 2013), the relationship between galaxy optical circular velocities and the circular velocities implied from their host haloes (Dutton et al. 2010), the halo baryonic mass function (Baldry et al. 2008), and the relation between central black hole mass and halo mass (Shankar et al. 2006). It has also been used to examine the dark matter haloes hosting certain types of galaxies, such as quasars (Croton 2009). Furthermore, abundance matching also allows the possibility of assigning observed galaxies at different redshifts to simulated haloes whose mass growth and merger history are known, allowing one to track the evolution of galaxies through time. This has been used to study the fate of satellite galaxies in clusters (Conroy et al. 2007), the frequency of gas-rich versus gas-poor mergers (Stewart et al. 2009b), the accuracy of observational indicators of halo mergers such as close pair counts (Stewart et al. 2009a), the evolution of the

* E-mail: akulier@princeton.edu

stellar-halo mass relation and velocity dispersion-halo mass relation and the implications for galaxy-halo co-evolution (Firmani & Avila-Reese 2010; Chae 2011), and the growth of Brightest Cluster Galaxies (Laporte et al. 2013), among many others.

However, a scheme that treats luminosity as the sole important property of a galaxy cannot be entirely correct. Galaxies are described by at least two parameters, as is apparent for moderate mass systems from the bimodal distribution of galaxy colors at fixed luminosity (e.g., Strateva et al. 2001; Blanton & Moustakas 2009). This implies that at least one other parameter of the galaxy’s halo, aside from its mass, must be relevant to the evolution of the galaxy.

Some recent work has explored the addition of another halo and galaxy parameter to abundance matching at fixed stellar and halo mass (Hearin & Watson 2013; Hearin et al. 2013; Watson et al. 2014); the authors refer to this scheme as “conditional abundance matching.” In Hearin & Watson (2013) and Hearin et al. (2013), the colors of galaxies are matched to a proxy for the halo age. The latter is parametrized as the earliest of three times: when the main halo progenitor mass exceeded $10^{12} M_{\odot}$, when the halo became a subhalo, or when the halo transitioned from fast to slow dark matter accretion, which is computed directly from the halo concentration as in Wechsler et al. (2002). In practice, the last, concentration-based, age parameter is the one used for all but the most massive galaxies. The authors find that their method is able to match a number of observables for galaxies separated into blue and red colors, including clustering statistics and the galaxy-galaxy lensing signal. Watson et al. (2014) apply the same method, but matching star formation rate (SFR) instead of galaxy color to halo age. They also report good agreement with observations, largely due to the correlation between SFR and galaxy color.

Even considering only massive early-type galaxies, one parameter is inadequate for predicting all of their properties. It has been known for some time that, while a rough one-parameter relation exists relating all variables to the velocity dispersion (the well-known “Faber-Jackson relation;” Faber & Jackson 1976), a two-dimensional parametrization called the “Fundamental Plane” (FP) offers a superior description (Dressler et al. 1987). An evolving FP has been detected from $z = 0$ out to $z \sim 2$ (van de Sande et al. 2014). Other properties of early-type galaxies, such as observed galaxy color, as well as modeled stellar population ages and metal abundances, have been found to be highly correlated with the FP parameters (Graves et al. 2009a,b; Graves & Faber 2010). This implies that the properties of early-type galaxies may be well-described by two parameters, making them a good sample on which to test a two-parameter matching scheme.

There are also other reasons why a two-parameter matching scheme may work best for massive early-type galaxies. The disk-to-bulge ratios of spiral galaxies are likely to be dependent on their environment (e.g., Hopkins et al. 2009). Also, galaxy color in star-forming galaxies will not be well-correlated with stellar age because a recent small burst of star formation can make a galaxy significantly bluer while only slightly changing the mean stellar population age.

One halo parameter of physical interest is the collapse time of the dark matter halo. That the properties of

galaxies hosted by dark matter haloes could be affected by variations in collapse time at fixed halo mass is an idea that has appeared in a number of previous works (e.g., Blumenthal et al. 1984). In particular, since the galaxy color of early-types should be well-correlated with the age of the stars in the galaxy (as well as their metallicity), it is possible that the galaxy color is also correlated with some measure of the collapse time of the host halo, which would determine when gas could collapse and form stars. There are also other galaxy parameters that are likely to be correlated with the collapse time of the host halo at fixed mass, such as the metallicity and stellar mass-to-light ratio. A present-day halo property correlated with the halo collapse time could then be matched with a present-day galaxy property as a second set of abundance matching parameters.

In this paper, we use a simple spherical collapse model to derive a present-day halo parameter that is a proxy for the halo collapse time. We adopt two different fitting functions for the $z = 0$ halo density profile, and also consider physical parameters that are independent of the function used to fit the halo profile. We will make use of the parameters we have found as part of a matching scheme to the Fundamental Plane in a future paper.

We first derive a proxy for halo collapse time using simple spherical collapse model in §2. We show the results of this model in §3. We compare our results with previous parametrizations of halo “formation time” (Bullock et al. 2001; Wechsler et al. 2002; Zhao et al. 2009) derived from dark matter simulations in §4. Finally, we describe a scheme for halo matching of the Fundamental Plane of elliptical galaxies (a two-parameter distribution), which is not obviously dependent on environment, that we plan to expand on in a future paper in §5.

In all parts of this paper we assume a cosmology consistent with the WMAP nine-year results plus external CMB, BAO, and H_0 measurements (Hinshaw et al. 2013, Table 4); thus we take $\Omega_{\Lambda,0} = 0.71$, $\Omega_{m,0} = 0.29$, and $H_0 = 69$ km/s/Mpc.

2 SPHERICAL COLLAPSE MODEL FOR HALO COLLAPSE TIME

We would like to choose some property of dark matter haloes that is a good proxy for the halo collapse time and can be easily measured in dark matter-only simulations. We approximate the collapse time of a dark matter perturbation early in the universe as twice the turnaround time in simple spherical models of collapse. We use a somewhat similar method to that of Rubin & Loeb (2013), who give equations for calculating the virialization density Δ_c for arbitrary pre-collapse and post-collapse density profiles by assuming mass and energy conservation. Our method is similar, except that we match the initial and final profiles within their turnaround radii at $z = 0$.

For the purposes of creating a two-parameter matching scheme, we choose final halo profiles that are described by two parameters and that are commonly used to fit numerically simulated haloes—namely, an NFW profile with parameters M_{200} and c , and a generalized NFW profile with varying mass M_{200} and inner slope α , with fixed $c = 5$ (see §2.2). We match these final profiles such that their mass M

and energy E within the shell that turns around at $z = 0$ is the same as that for chosen arbitrary initial profiles (e.g., tophat or Gaussian). While this model maps final profiles to initial profiles with two parameters uniquely (details below), the corresponding final profile is not actually the profile that the initial profile would evolve to, as evidenced by the fact that profiles of different shapes can be matched to the initial profiles this way. Rather, we choose final profiles that are used as approximations for a variety of dark matter halo profile shapes.

2.1 Initial Profile

Here we review the equations for the evolution of the initial profile; the analysis is similar to that in Mo et al. (2010).

We begin with some chosen initial overdensity profile $\rho_i(r_i)$ at arbitrarily chosen initial time t_i . We assume the profile will tend to the mean matter density of the universe at that time, $\bar{\rho}(t_i)$, for large radii. As long as the density is decreasing or constant with increasing radius, there will be no shell crossing for shells that have not yet collapsed and we can treat them separately. It is assumed that going far enough back in time, the initial perturbation is entirely expanding, and none of its shells have yet turned around. Also, in a Λ CDM universe, a finite amount of mass will collapse in an infinite time, because for overdensities lower than some value, the shells expand forever due to the Λ term instead of collapse. In the Appendix to this paper, we present an exact derivation of this value for an initial profile assumed to be on the Hubble flow, which tends toward the solution having $r = 0$ at $t = 0$ for $t_i \rightarrow 0$.

The collapse of each shell enclosing mass $M(< r)$ is governed by the following equation:

$$\frac{d^2 r}{dt^2} = -\frac{GM}{r^2} + \Omega_{\Lambda,0} H_0^2 r. \quad (1)$$

The above equation integrated once becomes

$$\frac{1}{2} \left(\frac{dr}{dt} \right)^2 - \frac{GM}{r} - \frac{\Omega_{\Lambda,0} H_0^2}{2} r^2 = \mathcal{E}, \quad (2)$$

where \mathcal{E} is the specific energy of the shell. At the turnaround time t_{ta} of a given shell, this becomes

$$\mathcal{E} = -\frac{GM}{r_{ta}} - \frac{\Omega_{\Lambda,0} H_0^2}{2} r_{ta}^2, \quad (3)$$

where the turnaround radius r_{ta} is the maximum radius attained by each shell. Defining

$$\zeta \equiv \frac{\Omega_{\Lambda,0} H_0^2 r_{ta}^3}{2GM}, \quad (4)$$

we see that for $\ddot{r} < 0$ at r_{ta} we require $\zeta < 1/2$. From this and Eqn. 2 we have a formula relating the radius of the shell and the time, as long as the shell has not yet turned around:

$$H_0 t = \left(\frac{\zeta}{\Omega_{\Lambda,0}} \right)^{1/2} \int_0^{r/r_{ta}} dx \left[\frac{1}{x} - 1 + \zeta(x^2 - 1) \right]^{-1/2}. \quad (5)$$

Using Eqn. 5, the central collapse time ($2 \times t_{ta}$) can be calculated for $r_{ta} \rightarrow 0$ (as long as the density profile does not have a central cusp), as can the time at which any fraction of the mass at $z = 0$ collapsed.

For a selected initial density profile $\rho(r_i)$ at time t_i , we

can find the energy of each shell from Eqn. 3. We first obtain r_{ta} for each r_i . To do that we re-express ζ as

$$\zeta = \frac{\Omega_{\Lambda,0} H_0^2}{\frac{8}{3} \pi G \rho_i(< r_i)} \left(\frac{r_{ta}}{r_i} \right)^3 \quad (6)$$

and insert into Eqn. 5 for $t_i(r_i)$. This can be solved numerically for r_{ta} as a function of t_i and r_i .

By setting t in Equation 5 to the age of the universe at $z = 0$ (referred to here as t_0) we can obtain ζ of the shell that is turning around at $z = 0$. Then we can use this same equation to find the ratio of the original radius to the turnaround radius r_i/r_{ta} of this shell by setting $t = t_i$. This combined with Equation 6 gives us the r_i and r_{ta} for the shell turning around at $z = 0$; we will designate these as $r_{i,max}$ and $r_{ta,max}$. We designate the mass and energy within $r_{i,max}$ at t_i (and $r_{ta,max}$ at t_0) as M_{tot} and E_{tot} , and these are what we will match to the mass and energy of the final profile. We also define the initial density within $r_{i,max}$ to be $\rho_{i,max}$, such that

$$r_{i,max} = \left(\frac{M_{tot}}{4/3 \pi \rho_{i,max}} \right)^{1/3}. \quad (7)$$

We can find \mathcal{E} for each shell using Eqn. 3. The total energy of all the shells within the maximum radius will then be

$$E_{tot} = \int_0^{r_{ta,max}} \mathcal{E}(r_{ta}) dM(r_{ta}). \quad (8)$$

To obtain $\mathcal{E}(r_{ta})$ for each shell at initial radius r_i between $r_i = 0$ and $r_i = r_{i,max}$, one can again insert Eqn. 6 into Eqn. 5 for $t = t_i$, and solve for r_{ta}/r_i .

Scaling the size of the profile by the radius $r_{i,max}$, so that the coordinate used is $y \equiv r/r_{i,max}$, Eqn. 3 gives

$$\mathcal{E} = -\frac{4}{3} \pi G \rho_i(< y) \frac{r_i}{r_{ta}} y^2 r_{i,max}^2 - \frac{\Omega_{\Lambda,0} H_0^2}{2} \left(\frac{r_{ta}}{r_i} \right)^2 y^2 r_{i,max}^2, \quad (9)$$

where r_{ta}/r_i is a function of y and also depends on z_0 and z_i .

Then, we can use Eqn. 6 to substitute for r_i/r_{ta} in the equation for \mathcal{E} ; we obtain:

$$\mathcal{E} = -\frac{1}{2} \left(\frac{8}{3} \pi G \right)^{2/3} \Omega_{\Lambda,0}^{1/3} H_0^{2/3} \rho_i^{2/3}(< y) \frac{1 + \zeta(y)}{\zeta^{1/3}(y)} y^2 r_{i,max}^2. \quad (10)$$

Then the total energy is then given by

$$\begin{aligned} E_{tot} &= \int \mathcal{E} dM = 4\pi r_{i,max}^3 \int_0^1 \mathcal{E}(y) \rho_i(y) y^2 dy \\ &= 4\pi r_{i,max}^5 \left[-\frac{1}{2} \left(\frac{8}{3} \pi G \right)^{2/3} \Omega_{\Lambda,0}^{1/3} H_0^{2/3} \times \right. \\ &\quad \left. \int_0^1 \rho_i^{2/3}(< y) \rho_i(y) \frac{1 + \zeta(y)}{\zeta^{1/3}(y)} y^4 dy \right], \end{aligned} \quad (11)$$

where using Eqn. 7 we then obtain

$$\begin{aligned} E_{tot}/M_{tot}^{5/3} &= -\frac{3}{\rho_{i,max}^{5/3}} \frac{1}{2^{1/3}} (H_0 G)^{2/3} \Omega_{\Lambda,0}^{1/3} \times \\ &\quad \int_0^1 \rho_i^{2/3}(< y) \rho_i(y) \frac{1 + \zeta(y)}{\zeta^{1/3}(y)} y^4 dy. \end{aligned} \quad (12)$$

This equation holds for any initial density profile $\rho_i(r_i)$ at any chosen z_i , as long as no part of the profile has yet collapsed.

For the initial profile, we also want to consider the limit as z_i becomes large. Here $\delta(< y)$, where $\rho_i(< y) = \bar{\rho}(z_i)(1 + \delta(< y))$, approaches (Mo et al. 2010):

$$\delta(< y) = \frac{3}{5} \frac{1 + \zeta(y)}{\zeta^{1/3}(y)} \left(\frac{\Omega_{\Lambda,0}}{\Omega_{m,0}} \right)^{1/3} (1 + z_i)^{-1}, \quad (13)$$

where ζ corresponds to a given turnaround (or collapse) time. We want to consider the same overdensity profile shape at all times; i.e., $\delta(< y)/\delta_{max}$ does not vary with time, where δ_{max} is the overdensity at $r_{i,max}$. It is clear that for a shell with a given collapse time, δ for that shell evolves with time; however, the above equation shows that for large z_i , a $\delta(y)/\delta_{max}$ profile taken to be constant with time is in fact also a constant profile in $\zeta(y)$ —that is, collapse time at any fixed interior mass.

Here $\rho_i(y)$ changes with z_i , but for large z_i , $\rho_i(y) \rightarrow \bar{\rho}(z_i)$ as the perturbation δ decreases like $(1 + z_i)^{-1}$ for fixed ζ (Eqn. 13), eliminating $\rho_{i,max}$, $\rho_i(< y)$, and $\rho_i(y)$. This gives

$$E_{tot}/M_{tot}^{5/3} = -\frac{3}{2^{1/3}} (H_0 G)^{2/3} \Omega_{\Lambda,0}^{1/3} \frac{1 + \zeta_0}{\zeta_0^{1/3}} \int_0^1 \frac{\delta(< y)}{\delta_{max}} y^4 dy, \quad (14)$$

where ζ_0 is the value of ζ for the shell that turns around at z_0 , in our case taken to be $z = 0$.

Since ζ_0 is dependent only on the reference redshift z_0 that we select and we assume that the overdensity profile is a constant shape, this expression approaches a constant value as $z_i \rightarrow \infty$. We see that $E/M^{5/3}$ is dependent only on the shape of the overdensity profile, which also determines the collapse times relative to the chosen reference redshift at high z_i . The lack of dependence on z_i for high z_i is due to the fact that Λ becomes unimportant at early times.

It is also clear that for a constant or decreasing overdensity profile, the integral on the right side of Equation 14 is bounded between 1/5 and 1/2, meaning that the energy within a shell turning around at a given redshift must be bounded between two values. However, as described in the next section, the final ($z = 0$) halo profiles we consider are common empirical fits to simulated haloes, and thus have unbounded possible values for $E/M^{5/3}$. Therefore, not all conceivable final profiles are able to correspond to a possible initial profile.

2.2 Final Profile

We would like to find a corresponding present-day halo density profile that has equal M_{tot} and E_{tot} within the turnaround radius at $z = 0$ ($t = t_0$) as the initial profile. We note that a specific turnaround time defines a unique density within the turnaround radius at that time (Eqns. 4 and 5), implying that for fixed M_{tot} , the final and initial profiles also have the same turnaround radius.

We choose two different forms for the present-day halo, based on the fact that these shapes are commonly used to fit simulated haloes:

- (i) The entire profile is described by an NFW profile over

the mean matter density:

$$\rho(r) = \frac{\rho_0}{r/r_s(1 + r/r_s)^2} + \bar{\rho}(t_0). \quad (15)$$

As noted above, for large values of the concentration c , $E/M^{5/3} \propto c/(\log c)^2$ for the NFW profile, which is not bounded. Therefore NFW profiles above some concentration cannot be the product of a simple spherical collapse model.

(ii) While the NFW profile is the most common parametrization of dark matter halo density, others have found that haloes are equally or better described by profiles that have a varying inner slope (e.g. Subramanian et al. 2000). In particular, Ricotti et al. (2007) have found that simulated dark matter haloes at virialization are equally well fit by either an NFW profile with varying c , or by a generalized NFW profile with fixed $c = 5$, and varying inner slope α . Thus we also match initial profiles to a dark matter density profile given by

$$\rho(r) = \frac{\rho_0}{(r/r_s)^\alpha(1 + r/r_s)^{3-\alpha}} + \bar{\rho}(t_0), \quad (16)$$

where r_s is related to M_{200} via the fixed concentration $c = 5$. We refer to this profile as an α model to avoid confusion with the NFW profile. This profile and the standard NFW have the same slope of -3 for large r , making their properties similar at large radii. As for the NFW profile, $E/M^{5/3}$ is unbounded for large α .

We assume haloes to be virialized within r_{200} , the radius within which the mean density is 200 times the critical density, and that the virial theorem can be used to find the energy within this region. Outside the virial radius, the profile is collapsing, out to a radius r_{ta} at which $t_{ta} = t_0$. While a different radius could be chosen within which the profile is virialized, we note that taking the virial radius to be r_{vir} as computed in Bryan & Norman (1998) would produce a negligible difference in our results.

The energy of the NFW profile within the radius turning around at $z = 0$ is the sum of the energy within the virial radius and the energy in the shells turning around. The potential energy within the virial radius is the sum of that from the matter and that from Λ :

$$U_m = - \int_0^{r_{200}} 4\pi \frac{GM(< r)}{r} \rho(r) r^2 dr, \quad (17)$$

$$U_\Lambda = - \int_0^{r_{200}} \frac{1}{2} \Omega_{\Lambda,0} H_0^2 4\pi \rho(r) r^4 dr, \quad (18)$$

and by the virial theorem, $E(r_{200}) = 0.5U_m + 2U_\Lambda$. Because $\bar{\rho}$ is much lower than the virial density, the fact that we take the density profile to be an NFW or an α model in overdensity has an insignificant effect on the virial energy we find within the virial radius. Thus the energies we obtain within the virial radius for the NFW profile are approximately those given by equations 3.33 and 4.20 in Rubin & Loeb (2013).

Outside the virial radius, the region between r_{200} and the turnaround radius r_{ta} is collapsing. To determine the energy for this region we use Eqn. 11. However, because the region is collapsing and not expanding, one must add the turnaround time to the time a shell has been collapsing

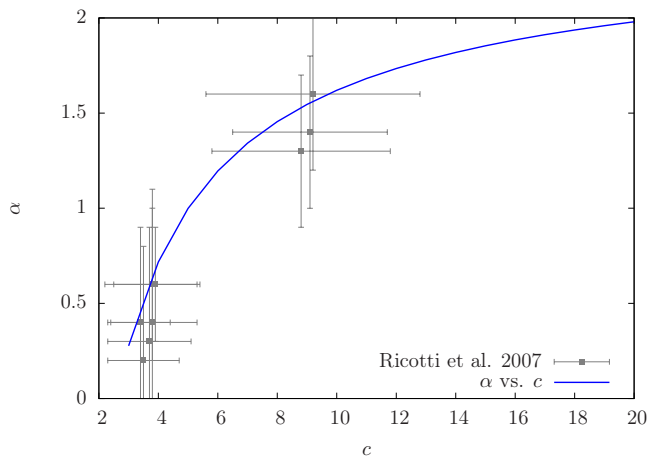


Figure 1. Correspondence between concentration c of NFW profiles and inner slope of α models, for profiles at $z = 0$ that have the same mass and energy within the turnaround radius. For comparison, gray points are from fits to simulated haloes from Ricotti et al. (2007), described in more detail in the text.

after t_{ta} , thus substituting Eqn. 5 with:

$$H_0 t_0 = \left(\frac{\zeta}{\Omega_{\Lambda,0}} \right)^{1/2} \left[\int_0^1 dx \left[\frac{1}{x} - 1 + \zeta(x^2 - 1) \right]^{-1/2} + \int_{r/r_{ta}}^1 dx \left[\frac{1}{x} - 1 + \zeta(x^2 - 1) \right]^{-1/2} \right]. \quad (19)$$

For a selected initial profile shape (e.g., a Gaussian) at a chosen initial time t_i , the above steps will create a one-to-one mapping between initial profiles with mass M_{tot} and energy E_{tot} and final profiles at $z = 0$ with the same mass and energy within the turnaround radius. Since both the NFW profiles and α model profiles are a two-parameter family, a unique combination of mass and energy values will correspond to a unique final profile of a given form.

3 RESULTS

Applying the above procedure, we are able to match final profiles to initial profiles. It is clear from Eqn. 12 that the value $E/M^{5/3}$ at a fixed redshift is dependent only on the shape of the overdensity profile (and the mean cosmic density at the chosen redshift), as it must be from dimensional arguments. For the final profiles we take to be at $z = 0$, NFW profiles and α models with the same mass and energy, this equation implies that there will be a relationship between c and α that is not mass-dependent. We show this relationship in Figure 1. More concentrated NFW profiles correspond to α model profiles with steeper inner slope. For comparison, we also show mean fits to the 40 most massive haloes from simulations at different redshifts from Ricotti et al. (2007). Our mapping using the energy and mass corresponds well to the match between α and c from direct fitting. This is as could be expected, since direct fitting ensures that the profiles will have similar shapes in the region $r \sim r_s$, and both profiles have slope -3 at large radii, leading to similar energies at fixed mass for both profile shapes.

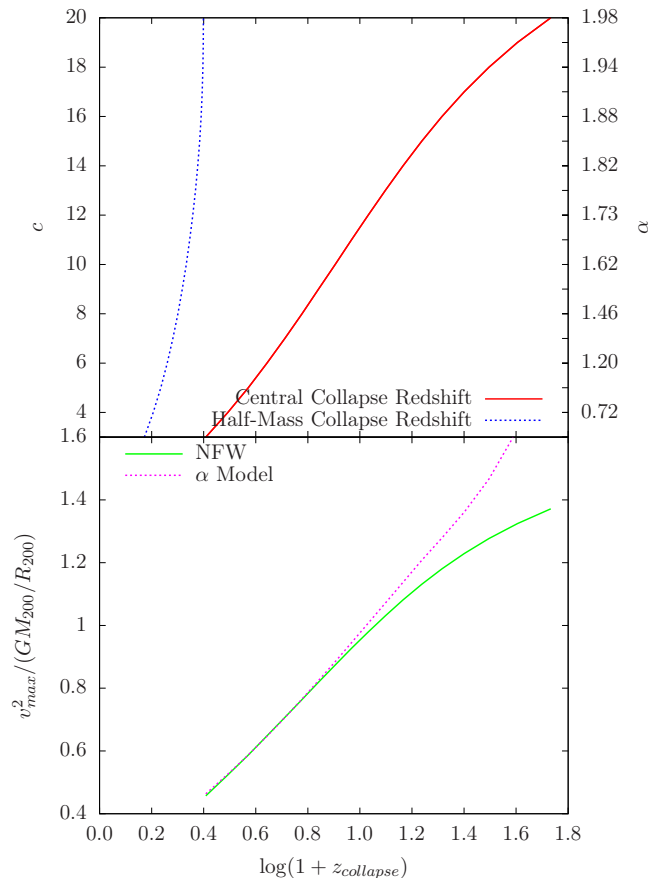


Figure 2. Top Panel: The concentration c of final NFW profiles, or inner slope α of α models, for different central and half-mass collapse redshifts of initial Gaussian overdensity profiles at $z_i = 1000$. The matching between initial and final profiles is described in the text. The $z = 0$ halo concentration (or alternatively, inner slope) is monotonically and positively correlated with the collapse redshift of any fraction of the $z = 0$ mass.

Bottom Panel: The normalized squared maximum circular velocity, $v_{max}^2/(GM_{200}/R_{200})$, at $z = 0$ for an NFW profile with varying c , and an α model with varying inner slope α , versus the central collapse redshift of the matching initial Gaussian overdensity profile with $z_i = 1000$. The range in c and α shown is the same as in the top panel. The similarity in $v_{max}^2/(GM_{200}/R_{200})$ for NFW profiles and α models over the range of physical interest is apparent.

Similarly, Equation 12 implies that for the initial profiles, $E/M^{5/3}$ is also a function of only the shape of the overdensity profile and the mean density at the chosen initial redshift z_i . Furthermore, as seen in Equation 14, for a fixed overdensity shape, the value of $E/M^{5/3}$ approaches a constant value as $z_i \rightarrow \infty$. However, the collapse time for a mass shell containing a certain fraction of the total mass is also a function of only the chosen initial redshift z_i and the shape of the overdensity profile (Equations 5 and 6), and also approaches a constant value for fixed overdensity shape as $z_i \rightarrow \infty$ (Equation 13). Thus the value of c or α of the final profile will be a function of the collapse time of any chosen fraction of the mass for an initial profile of a fixed shape for fixed z_i . We show this correspondence in the top panel of Figure 2, in which we present the NFW concentration c (or

α model inner slope) versus the collapse time of the center of an initial Gaussian profile, as well as the time for half the mass collapsed at $z = 0$ of the initial profile to collapse. For the initial profile we take $z_i = 1000$ and compute the exact collapse times as described in §2.1; however, this redshift is large enough that the results will be similar to those calculated with the approximation of $z_i \rightarrow \infty$. We find that more concentrated haloes (or those with steeper α) have earlier collapse times, as might have been intuitively expected. Thus, either α or c can be used as a proxy monotonically related to collapse epoch that is independent of halo mass.

The results depend on the choice of initial profile. They also depend (weakly) on z_i , the initial redshift at which the profile is selected to be the shape of choice. This is because in general the shape of the profile evolves over time, so that the same profile at a later or earlier time does not follow the same functional form. Thus the dependence on z_i can also be seen as equivalent to a dependence on the shape of the profile at any given time. However, as seen in §2.1, as $z_i \rightarrow \infty$, the dependence on z_i disappears, and the value of $E/M^{5/3}$ depends only on the overdensity profile shape.

Additionally, we present two tables showing the same values as the top panel of Figure 2; Tables 1 and 2 show the central and half mass collapse time, respectively, for NFW profiles with concentration c and mass M_{200} . While the collapse times do not depend on M_{200} , in bold we show the mass-concentration relation for simulated dark matter haloes from Diemer & Kravtsov (2014), in an observationally normalized CDM universe within which both typical values of c and M_{200} are functions of collapse epoch. We select the results from Diemer & Kravtsov (2014) that use the same cosmology as we assume throughout the paper (Hinshaw et al. 2013). The range in c at fixed mass represents their reported one-sigma scatter of 0.16 dex. By nature, our calculation is done for an arbitrary initial profile, so we do not assume cosmological initial conditions. Thus we must take the mass-concentration relation from elsewhere. For the assumptions about the initial profile we have made above, the bold values represent the expected scatter in the central and half-mass collapse redshifts for NFW profiles of a given virial mass. The ratio of the actual concentration of a halo to the mean concentration of haloes of its virial mass, $c/\bar{c}(M_{200})$, could be used as a parameter in a two-parameter matching scheme between haloes and galaxies that would be correlated with the halo collapse time and potentially with galaxy properties at fixed mass, as described in our discussion of future work in §5.

The bottom panel of Figure 2 shows another parameter of the final profile, the normalized squared maximum circular velocity $v_{max}^2/(GM_{200}/R_{200})$, versus the central collapse redshift of the same initial profile as in the top panel. Again, as can be expected from dimensional arguments, this parameter is a function of the collapse redshift. We compare the circular velocity of the final NFW and corresponding α model profiles. The values are similar at low circular velocity (low c or α) and diverge for high circular velocity, but are close to one another for the relevant range of circular velocity values seen in dark matter haloes. Thus $v_{max}^2/(GM_{200}/R_{200})$ could also potentially be used as a parameter in a halo matching scheme, and would have the benefit of not being highly dependent on the fitting function chosen for the dark matter halo profile.

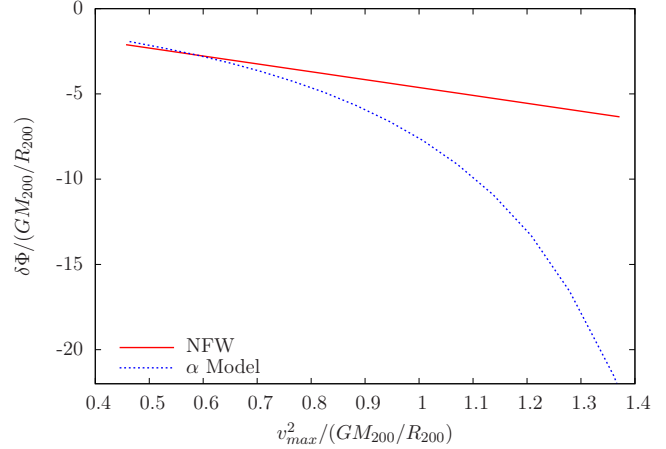


Figure 3. The normalized squared maximum circular velocity, $v_{max}^2/(GM_{200}/R_{200})$, versus the normalized excess central potential, $\delta\Phi/(GM_{200}/R_{200})$, at $z = 0$ for an NFW profile with varying c and an α model with varying inner slope α . Unlike the maximum circular velocity shown in Figure 2, the central potential is significantly different for the two models.

In Figure 3, we show the $v_{max}^2/(GM_{200}/R_{200})$ versus a related parameter, the excess normalized central potential $\delta\Phi/(GM_{200}/R_{200})$, for both NFW profiles and α models. While the values of $v_{max}^2/(GM_{200}/R_{200})$ are similar for both models at fixed mass and energy, the values of the central potential are significantly different for the two profiles shapes, implying that the maximum circular velocity is a superior “common” parameter between the two types of models to use to predict the initial halo collapse redshift.

For reference, we show contours of constant v_{max} in Figure 4, in the top panel for varying M_{200} and c for NFW profiles, and in the bottom panel for varying M_{200} and α for α models, over the range of physical interest.

4 COMPARISON TO PREVIOUS WORK

Previous papers have investigated parametrizations of the time at which a halo formed, usually based on the results of dark matter simulations. Such papers include Bullock et al. (2001) and Wechsler et al. (2002). The model of Wechsler et al. (2002) improved upon that of Bullock et al. (2001), but obtained similar results.

Wechsler et al. (2002) examined the mass accretion histories of the most massive progenitors of individual haloes from dark matter simulations for $z < 7$, defining the halo mass to be the mass within Δ_{vir} (Bryan & Norman 1998). Wechsler et al. (2002) found that the mass accretion histories of haloes at each timestep, despite halo mergers in the simulation, can generally be fit well by a simple analytic form:

$$M(a) = M_0 \exp \left[-a_c S \left(\frac{a_0}{a} - 1 \right) \right]. \quad (20)$$

Here a is the scale factor, a_0 is a reference scale factor at which the mass of the halo is M_0 , S is an arbitrarily chosen constant, and a_c is taken to be the “formation scale factor” of the halo, given the choice of S . This form is self-consistent for different choices of a_0 . Taking the formation scale factor

Table 1. Central collapse redshifts for an initial Gaussian profile at $z_i = 1000$. This table shows the central collapse redshifts of initial Gaussians matched to NFW profiles with varying M_{200} and c . Bold numbers indicate the one-sigma scatter around the $z = 0$ mass-concentration relation for NFWs from Diemer & Kravtsov (2014).

c	$M_{200} [M_{\odot}]$								
	1.00e+10	2.51e+10	6.31e+10	1.58e+11	3.98e+11	1.00e+12	2.51e+12	6.31e+12	1.58e+13
3.0	1.56e+00	1.56e+00	1.56e+00	1.56e+00	1.56e+00	1.56e+00	1.56e+00	1.56e+00	1.56e+00
4.0	2.11e+00	2.11e+00	2.11e+00	2.11e+00	2.11e+00	2.11e+00	2.11e+00	2.11e+00	2.11e+00
5.0	2.73e+00	2.73e+00	2.73e+00	2.73e+00	2.73e+00	2.73e+00	2.73e+00	2.73e+00	2.73e+00
6.0	3.40e+00	3.40e+00	3.40e+00	3.40e+00	3.40e+00	3.40e+00	3.40e+00	3.40e+00	3.40e+00
7.0	4.15e+00	4.15e+00	4.15e+00	4.15e+00	4.15e+00	4.15e+00	4.15e+00	4.15e+00	4.15e+00
8.0	5.00e+00	5.00e+00	5.00e+00	5.00e+00	5.00e+00	5.00e+00	5.00e+00	5.00e+00	5.00e+00
9.0	5.94e+00	5.94e+00	5.94e+00	5.94e+00	5.94e+00	5.94e+00	5.94e+00	5.94e+00	5.94e+00
10.0	7.04e+00	7.04e+00	7.04e+00	7.04e+00	7.04e+00	7.04e+00	7.04e+00	7.04e+00	7.04e+00
11.0	8.29e+00	8.29e+00	8.29e+00	8.29e+00	8.29e+00	8.29e+00	8.29e+00	8.29e+00	8.29e+00
12.0	9.76e+00	9.76e+00	9.76e+00	9.76e+00	9.76e+00	9.76e+00	9.76e+00	9.76e+00	9.76e+00
13.0	1.15e+01	1.15e+01	1.15e+01	1.15e+01	1.15e+01	1.15e+01	1.15e+01	1.15e+01	1.15e+01
14.0	1.36e+01	1.36e+01	1.36e+01	1.36e+01	1.36e+01	1.36e+01	1.36e+01	1.36e+01	1.36e+01
15.0	1.63e+01	1.63e+01	1.63e+01	1.63e+01	1.63e+01	1.63e+01	1.63e+01	1.63e+01	1.63e+01
16.0	1.97e+01	1.97e+01	1.97e+01						
17.0	2.42e+01	2.42e+01	2.42e+01						
18.0	3.03e+01	3.03e+01							
19.0	3.93e+01	3.93e+01							
20.0	5.31e+01	5.31e+01	5.31e+01	5.31e+01	5.31e+01	5.31e+01	5.31e+01	5.31e+01	5.31e+01

Table 2. Half-mass collapse redshifts for an initial Gaussian profile at $z_i = 1000$. Same as Table 1, but for the half-mass collapse redshift.

c	$M_{200} [M_{\odot}]$								
	1.00e+10	2.51e+10	6.31e+10	1.58e+11	3.98e+11	1.00e+12	2.51e+12	6.31e+12	1.58e+13
3.0	4.87e-01	4.87e-01	4.87e-01	4.87e-01	4.87e-01	4.87e-01	4.87e-01	4.87e-01	4.87e-01
4.0	6.07e-01	6.07e-01	6.07e-01	6.07e-01	6.07e-01	6.07e-01	6.07e-01	6.07e-01	6.07e-01
5.0	7.18e-01	7.18e-01	7.18e-01	7.18e-01	7.18e-01	7.18e-01	7.18e-01	7.18e-01	7.18e-01
6.0	8.19e-01	8.19e-01	8.19e-01	8.19e-01	8.19e-01	8.19e-01	8.19e-01	8.19e-01	8.19e-01
7.0	9.12e-01	9.12e-01	9.12e-01	9.12e-01	9.12e-01	9.12e-01	9.12e-01	9.12e-01	9.12e-01
8.0	9.99e-01	9.99e-01	9.99e-01	9.99e-01	9.99e-01	9.99e-01	9.99e-01	9.99e-01	9.99e-01
9.0	1.08e+00	1.08e+00	1.08e+00	1.08e+00	1.08e+00	1.08e+00	1.08e+00	1.08e+00	1.08e+00
10.0	1.15e+00	1.15e+00	1.15e+00	1.15e+00	1.15e+00	1.15e+00	1.15e+00	1.15e+00	1.15e+00
11.0	1.22e+00	1.22e+00	1.22e+00	1.22e+00	1.22e+00	1.22e+00	1.22e+00	1.22e+00	1.22e+00
12.0	1.28e+00	1.28e+00	1.28e+00	1.28e+00	1.28e+00	1.28e+00	1.28e+00	1.28e+00	1.28e+00
13.0	1.34e+00	1.34e+00	1.34e+00	1.34e+00	1.34e+00	1.34e+00	1.34e+00	1.34e+00	1.34e+00
14.0	1.38e+00	1.38e+00	1.38e+00	1.38e+00	1.38e+00	1.38e+00	1.38e+00	1.38e+00	1.38e+00
15.0	1.42e+00	1.42e+00	1.42e+00	1.42e+00	1.42e+00	1.42e+00	1.42e+00	1.42e+00	1.42e+00
16.0	1.46e+00	1.46e+00	1.46e+00						
17.0	1.48e+00	1.48e+00	1.48e+00						
18.0	1.49e+00	1.49e+00							
19.0	1.50e+00	1.50e+00							
20.0	1.50e+00	1.50e+00	1.50e+00	1.50e+00	1.50e+00	1.50e+00	1.50e+00	1.50e+00	1.50e+00

a_c of the halo as defined above with S chosen to be 2, the authors assign a formation time to each halo and find that the concentration of each halo at some reference scale factor a_0 is related to the formation time via

$$c_{\text{vir}} = 4.1a_0/a_c \quad (21)$$

where the constant 4.1 is the concentration of haloes “forming” at the present day, given the choice of $S = 2$.

A more recent paper looking at mass accretion histories in dark matter simulations is Zhao et al. (2009). The authors claim to obtain more accurate fits to halo accretion histories using a more complex model than Wechsler et al. (2002) and Bullock et al. (2001). Unlike Wechsler et al. (2002), they find that mass accretion histories follow a power-law form as opposed to an exponential. Zhao et al. (2009) find that the concentration of haloes at some observation time t is a function of the time at which their mass reached 4% of the mass at the observation time, given by

$$c = [4^8 + (t/t_{0.04})^{8.4}]^{1/8} \quad (22)$$

where $t_{0.04}$ is the time at which 4% of the mass at t was

reached. Note that halo concentrations in this model cannot be less than 4.

Due to the fact that we begin with arbitrary initial conditions and not cosmological ones, it is difficult to compare our results with those of Wechsler et al. (2002) and Zhao et al. (2009). However, both our model and the results obtained by these two papers find a monotonic relation between the collapse time or “formation time” of haloes and their concentrations at fixed mass at any given time, where a higher concentration implies an earlier formation time. This is crucial as abundance matching-type methods require a monotonic relation between the parameters being matched.

5 FUTURE WORK

Using a combination of two halo parameters, one can perform two-parameter abundance matching to two observable parameters of galaxies. As shown above, parameters that correlate well with the physically relevant parameter of halo collapse time include c or α , or alternatively

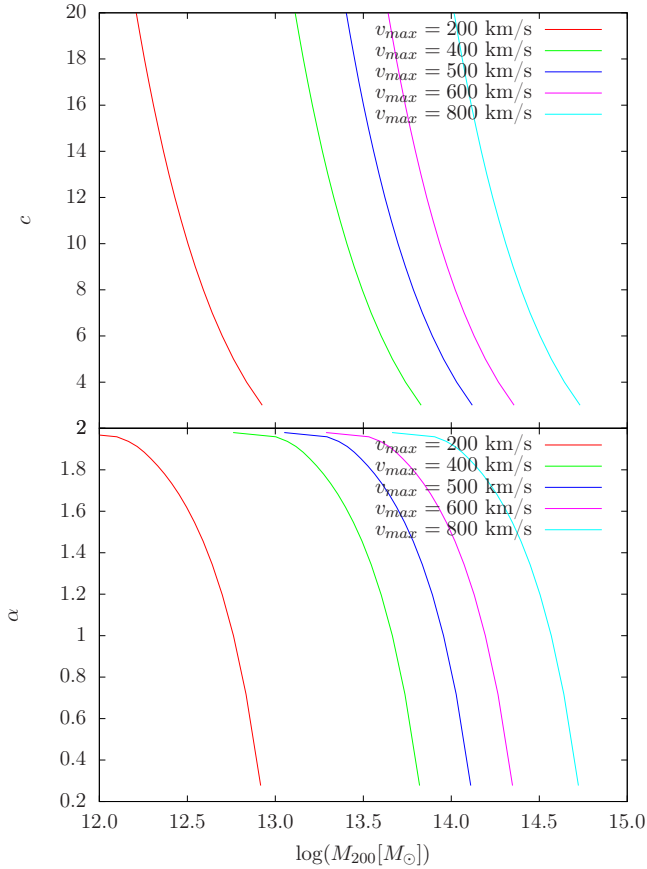


Figure 4. Contours of constant v_{max} for varying M_{200} and c for NFW profiles in the top panel, and the same for varying M_{200} and inner slope for α models in the bottom panel.

$v_{max}^2/(GM_{200}/R_{200})$. These could be combined with the parameter M_{200} used in standard abundance matching, although these are not the only possible choices for matching.

Because we only consider two parameters, and standard abundance matching is most effective for massive galaxies, we plan to focus on two-parameter abundance matching to the Fundamental Plane of massive early type galaxies in future work. The Fundamental Plane is an observed relationship between three parameters: the effective radius R_e , the velocity dispersion σ , and the surface brightness within R_e , I_e (or alternatively, the luminosity within R_e). Elliptical galaxies occupy a plane in the space of these three parameters:

$$\log R_e = a \log \sigma + b \log I_e + c_z, \quad (23)$$

where a and b are constants and c_z is a redshift-dependent zero-point. Assuming that the mass-to-light ratio of elliptical galaxies is roughly independent of stellar mass, and that the galaxies are fully virialized, one would expect from the virial theorem that the fundamental plane would follow $R_e \propto \sigma^2 I_e^{-1}$. However, the observed fundamental plane has a tilt with respect to this relation (e.g., Bezanson et al. 2013). Although the FP has some thickness and is not completely two-dimensional, this thickness is small (Graves et al. 2009b; Graves & Faber 2010). While we plan to focus on early-type galaxies, interestingly, Bezanson et al. (2014) find that

early- and late-type galaxies fall on the same mass fundamental plane.

Additionally, other galactic parameters have been found to be strongly correlated with parameters of the Fundamental Plane. These include galaxy color, stellar mass-to-light ratio, and mean stellar population age and metallicity (Graves et al. 2009a,b; Graves & Faber 2010; Porter et al. 2014). Thus matching to the FP would take into account the variance in these parameters as well, potentially allowing a near-complete prediction of the properties of a massive galaxy residing in a halo based off the halo’s properties, and creating a better connection between the properties of the halo (including formation epoch) and the properties of the galaxy.

ACKNOWLEDGMENTS

We thank Sandra Faber, Alexie Leauthaud, and Renyue Cen for their comments on the paper. A.K. was supported by the National Science Foundation Graduate Research Fellowship, Grant No. DGE-1148900.

REFERENCES

- Baldry I. K., Glazebrook K., Driver S. P., 2008, MNRAS, 388, 945
 Behroozi P. S., Conroy C., Wechsler R. H., 2010, ApJ, 717, 379
 Bezanson R., Franx M., van Dokkum P., 2014, ArXiv e-prints
 Bezanson R., van Dokkum P. G., van de Sande J., Franx M., Leja J., Kriek M., 2013, ApJ, 779, L21
 Blanton M. R., Moustakas J., 2009, ARA&A, 47, 159
 Blumenthal G. R., Faber S. M., Primack J. R., Rees M. J., 1984, Nature, 311, 517
 Bryan G. L., Norman M. L., 1998, ApJ, 495, 80
 Bullock J. S., Kolatt T. S., Sigad Y., Somerville R. S., Kravtsov A. V., Klypin A. A., Primack J. R., Dekel A., 2001, MNRAS, 321, 559
 Chae K.-H., 2011, MNRAS, 413, 887
 Conroy C., Wechsler R. H., 2009, ApJ, 696, 620
 Conroy C., Wechsler R. H., Kravtsov A. V., 2006, ApJ, 647, 201
 Conroy C., Wechsler R. H., Kravtsov A. V., 2007, ApJ, 668, 826
 Croton D. J., 2009, MNRAS, 394, 1109
 Diemer B., Kravtsov A. V., 2014, ApJ, 789, 1
 Dressler A., Lynden-Bell D., Burstein D., Davies R. L., Faber S. M., Terlevich R., Wegner G., 1987, ApJ, 313, 42
 Dutton A. A., Conroy C., van den Bosch F. C., Prada F., More S., 2010, MNRAS, 407, 2
 Faber S. M., Jackson R. E., 1976, ApJ, 204, 668
 Firmani C., Avila-Reese V., 2010, ApJ, 723, 755
 Fosalba P., Gaztañaga E., Castander F. J., Crocce M., 2015, MNRAS, 447, 1319
 Graves G. J., Faber S. M., 2010, ApJ, 717, 803
 Graves G. J., Faber S. M., Schiavon R. P., 2009a, ApJ, 693, 486
 Graves G. J., Faber S. M., Schiavon R. P., 2009b, ApJ, 698, 1590

- Gunn J. E., Gott, III J. R., 1972, *ApJ*, 176, 1
Guo Q., White S., Li C., Boylan-Kolchin M., 2010, *MNRAS*, 404, 1111
Hearin A. P., Watson D. F., 2013, *MNRAS*, 435, 1313
Hearin A. P., Watson D. F., Becker M. R., Reyes R., Berlind A. A., Zentner A. R., 2013, *ArXiv e-prints*
Hinshaw G. et al., 2013, *ApJS*, 208, 19
Hopkins P. F., Cox T. J., Younger J. D., Hernquist L., 2009, *ApJ*, 691, 1168
Kravtsov A. V., Berlind A. A., Wechsler R. H., Klypin A. A., Gottlöber S., Allgood B., Primack J. R., 2004, *ApJ*, 609, 35
Laporte C. F. P., White S. D. M., Naab T., Gao L., 2013, *MNRAS*, 435, 901
Leauthaud A. et al., 2012, *ApJ*, 746, 95
Mo H., van den Bosch F. C., White S., 2010, *Galaxy Formation and Evolution*
Moster B. P., Naab T., White S. D. M., 2013, *MNRAS*, 428, 3121
Nuza S. E. et al., 2013, *MNRAS*, 432, 743
Porter L. A., Somerville R. S., Primack J. R., Croton D. J., Covington M. D., Graves G. J., Faber S. M., 2014, *ArXiv e-prints*
Ricotti M., Pontzen A., Viel M., 2007, *ApJ*, 663, L53
Rubin D., Loeb A., 2013, *JCAP*, 12, 19
Shankar F., Lapi A., Salucci P., De Zotti G., Danese L., 2006, *ApJ*, 643, 14
Stewart K. R., Bullock J. S., Barton E. J., Wechsler R. H., 2009a, *ApJ*, 702, 1005
Stewart K. R., Bullock J. S., Wechsler R. H., Maller A. H., 2009b, *ApJ*, 702, 307
Strateva I. et al., 2001, *AJ*, 122, 1861
Subramanian K., Cen R., Ostriker J. P., 2000, *ApJ*, 538, 528
Vale A., Ostriker J. P., 2004a, *MNRAS*, 353, 189
Vale A., Ostriker J. P., 2004b, *MNRAS*, 353, 189
van de Sande J., Kriek M., Franx M., Bezanson R., van Dokkum P. G., 2014, *ApJ*, 793, L31
Wake D. A. et al., 2011, *ApJ*, 728, 46
Watson D. F., Hearin A. P., Berlind A. A., Becker M. R., Behroozi P. S., Skibba R. A., Reyes R., Zentner A. R., 2014, *ArXiv e-prints*
Wechsler R. H., Bullock J. S., Primack J. R., Kravtsov A. V., Dekel A., 2002, *ApJ*, 568, 52
Zhao D. H., Jing Y. P., Mo H. J., Börner G., 2009, *ApJ*, 707, 354

APPENDIX

In §2.1, we show the equations determining the evolution of mass shells of an overdensity in a Λ CDM universe, where each shell has initial condition $r = 0$ at $t = 0$. In a Λ CDM universe, mass shells with overdensity δ below some value will never turn around. For the case presented in §2.1, there is no simple analytic formula for this overdensity for all times (although it can be found numerically from the equations given therein), but there is one as the initial time approaches 0, given by Eqn. 13. However, for the case in which all mass shells are taken to be initially on the Hubble flow (i.e., $\dot{r}_i = H_i(t_i)r_i$ for a chosen initial time t_i), there is an analytic solution for the minimum overdensity to turn around for all

initial times. Here we present a short derivation of this value and compare to the solution for initial conditions $r = 0$ at $t = 0$ at early times.

Once again, we begin with the equation of motion for a shell containing mass M :

$$\frac{d^2r}{dt^2} = -\frac{GM}{r^2} + \Omega_{\Lambda,0}H_0^2r. \quad (24)$$

Integrated once, we obtain

$$\frac{1}{2}\dot{r}^2 - \frac{1}{2}\dot{r}_i^2 = \frac{GM}{r} - \frac{GM}{r_i} + \frac{\Omega_{\Lambda,0}H_0^2}{2}r^2 - \frac{\Omega_{\Lambda,0}H_0^2}{2}r_i^2. \quad (25)$$

Here our initial condition is

$$\dot{r}_i^2 = H_i^2r_i^2 = \frac{2G\langle M \rangle}{r_i} + \Omega_{\Lambda,0}H_0^2r_i^2, \quad \langle M \rangle \equiv \frac{4}{3}\pi G\bar{\rho}(t_i)r_i^3. \quad (26)$$

Combined with Eqn. 25, we obtain

$$\dot{r}^2 = \frac{2GM}{r} + \Omega_{\Lambda,0}H_0^2r^2 - \frac{2G(M - \langle M \rangle)}{r_i}. \quad (27)$$

Now we define

$$r/r_i \equiv \chi, \quad \frac{d}{dt} \equiv H_i \frac{d}{d\tau} \quad (28)$$

giving

$$\left(\frac{d\chi}{d\tau}\right)^2 = \frac{8\pi G\bar{\rho}}{3H_i^2} \frac{M}{\langle M \rangle} \frac{1}{\chi} + \frac{\Omega_{\Lambda,0}H_0^2}{H_i^2} \chi^2 - \frac{8\pi G\bar{\rho}}{3H_i^2} \frac{M - \langle M \rangle}{\langle M \rangle}. \quad (29)$$

Noting that

$$1 + \delta = \frac{M}{\langle M \rangle}, \quad \frac{8\pi G\bar{\rho}}{3H_i^2} = \Omega_{m,i}, \quad \frac{\Omega_{\Lambda,0}H_0^2}{H_i^2} = \Omega_{\Lambda,i} \quad (30)$$

and that for a flat universe $\Omega_{m,i} + \Omega_{\Lambda,i} = 1$, we obtain

$$\left(\frac{d\chi}{d\tau}\right)^2 = \frac{\Omega_{m,i}(1 + \delta)}{\chi} + \Omega_{\Lambda,i}\chi^2 - \Omega_{m,i}\delta. \quad (31)$$

For any shell that turns around, $(d\chi/d\tau)^2 = 0$ for some maximal value of χ . Therefore we want to find the smallest δ such that there exists a positive χ where

$$\chi^3 - \frac{\Omega_{m,i}}{\Omega_{\Lambda,i}}\delta\chi + \frac{\Omega_{m,i}}{\Omega_{\Lambda,i}}(1 + \delta) = 0. \quad (32)$$

We also require that this cubic to be positive for χ between 0 and the maximum value of χ in order for $d\chi/d\tau$ to be a real number. This cubic has inflection points at $\chi_{\pm} = \pm(\Omega_{m,i}\delta/3\Omega_{\Lambda,i})^{1/2}$; for the previously mentioned conditions to hold, it requires that the value of the cubic at χ_+ be negative or 0:

$$\left(\frac{\Omega_{m,i}}{\Omega_{\Lambda,i}}\frac{\delta}{3}\right)^{3/2} - \frac{1}{3^{1/2}}\left(\frac{\Omega_{m,i}}{\Omega_{\Lambda,i}}\delta\right)^{3/2} + \frac{\Omega_{m,i}}{\Omega_{\Lambda,i}}(1 + \delta) \leq 0. \quad (33)$$

This reduces to simply

$$\frac{\delta^3}{(1 + \delta)^2} \geq \frac{27}{4} \frac{\Omega_{m,i}}{\Omega_{\Lambda,i}}. \quad (34)$$

As stated, this is the exact solution for an initial profile that is assumed to be on the Hubble flow at time t_i . This can be compared to Equation 13, which is the solution for δ with initial conditions $r = 0$ at $t = 0$ for all shells as $z_i \rightarrow \infty$. Here the boundary between collapsing and forever expanding shells is given by $\zeta = 0.5$, by the definition of ζ . This gives for the minimal overdensity at early times

$$\delta = \frac{9}{10} 2^{1/3} \left(\frac{\Omega_{m,i}}{\Omega_{\Lambda,i}}\right)^{1/3}; \quad (35)$$

whereas at early times for the solution on the Hubble flow we find

$$\delta \approx \frac{3}{2} 2^{1/3} \left(\frac{\Omega_{m,i}}{\Omega_{\Lambda,i}} \right)^{1/3}. \quad (36)$$

It can be seen that the derived δ differs by a value of $3/5$. This is the difference in overdensity expected for a matter-dominated universe between considering a hypersurface of constant H_i and one of constant t_i , as derived in Gunn & Gott (1972). This ratio between the results will not hold at small z_i due to the effect of Λ , but for early times the universe is increasingly matter dominated and so the two solutions are the same modulo this factor of $3/5$.